



OPEN Histomorphometric and microtomographic evaluation of hydroxyapatite coated implants and L-PRF in over drilled bone sites in sheep

Sylvio Luiz Costa De-Moraes¹, Fernando Cesar Amazonas Lima¹, Suelen Cristina Sartoretto^{2,3}, Bruna Ghiraldini⁴, Fabio Jose Barbosa Bezerra⁵, Pamella Santana Nunes¹, Caio Márcio Sorrentino de Freitas Farias dos Santos⁶, Monica Diuana Calasans-Maia² & Jose Mauro Granjeiro^{2,7}✉

Hydroxyapatite used as a coating for titanium dental implants reduces the time required for osseointegration. Platelet-rich fibrin (L-PRF) releases growth factors and cytokines, enhancing tissue healing and bone regeneration. This study aimed to evaluate histologically, histomorphometrically, and by microcomputed tomography an implant surface coated with nanostructured hydroxyapatite (HANano), in comparison with a double acid-etched (DAA) surface, both with and without peri-implant grafting with L-PRF, installed in over-instrumented sites in a low-density bone. Five adult sheep (2–4 years old) received twenty 3.5 × 10 mm implants in the iliac crest. Bone-to-implant contact (BIC) and bone-occupied area fraction (BAFo) were evaluated histomorphometrically after an 8-week experimental period. Brown-Forsyth analysis of variance (ANOVA) and Welch's ANOVA test did not identify significant differences between the experimental groups. On average, BIC ranged from 44% (HANano + L-PRF) to 63% (DAA + L-PRF). μ CT analysis revealed that bone volume density in the peri-implant region ranged from 26% (HANano + L-PRF) to 39% (DAA). No statistically significant differences were observed between the groups. Both implant surfaces studied allowed osseointegration in low bone density sites, independently of peri-implant grafting with L-PRF, after 8 weeks of implantation. While this model provided controlled conditions for evaluating early-stage osseointegration, the absence of functional loading and the relatively short follow-up period should be considered when extrapolating the findings to clinical applications. Future studies should assess these variables under load-bearing conditions with extended observation periods. All the sheep in this study remained alive.

Keywords Titanium dental implants, Osseointegration, Hydroxyapatite, Double acid attack, Sheep, L-PRF

Titanium is a biocompatible material that enables osseointegration by promoting tissue healing without triggering foreign body reactions, while also facilitating cellular responses essential for the repair process¹. Advances in surface treatments have led to the replacement of machined or minimally rough titanium implants with treated surfaces, enhancing predictability, survival rates, and osseointegration efficiency^{2–5}.

The long-term stability of dental implants depends on implant-related and non-implant-related factors. Non-implant-related factors include the patient health, receptor site quality, surgical technique, and loading

¹Post-Graduation Program in Dentistry, Fluminense Federal University, Niteroi 24220-140, Brazil. ²Clinical Research Laboratory, Dentistry School, Universidade Federal Fluminense, Niteroi 24220-140, Brazil. ³Oral Surgery Department, Fluminense Federal University, Niteroi 24220-140, Brazil. ⁴Dental Research Division, Dentistry School, Universidade Paulista, São Paulo 04710-000, Brazil. ⁵Oral Surgery and Periodontology Department, São Paulo University, Ribeirão Preto 14040-904, Brazil. ⁶Coordination of Condensed Matter, Applied Physics and Nanoscience - Brazilian Center for Physics Research (COMAN - CBPF), Dr. Xavier Sigaud, 150 - Botafogo, Rio de Janeiro 22290-180, Brazil. ⁷National Institute of Metrology, Quality and Technology (INMETRO), Duque de Caxias 25250-020, Brazil. ✉email: jmgranjeiro@gmail.com

conditions⁶. Implant-related factors primarily involve implant macrogeometry and surface characteristics at the micro- and nanoscale, which are modified via surface treatments to enhance biological interactions⁷.

Hydroxyapatite (HA), a calcium phosphate compound, is one of dentistry's most extensively studied and applied bioceramics due to its biological and crystallographic similarities to bone tissue⁸. HA comprises approximately 67% of the bone matrix⁹ and is recognized for its biocompatibility and bioactivity, stimulating bone formation around implants and facilitating osseointegration⁹. HA is commonly used as a titanium implant coating, demonstrating positive effects on osseointegration, inflammatory response regulation, and antibacterial activity¹⁰.

Histologically, osseointegration is defined as the direct anchorage of an implant to bone, characterized by new bone formation in direct contact with the implant surface, without fibrous tissue interposition¹¹. Enhancing and accelerating osseointegration is crucial for early implant loading, allowing for faster masticatory function restoration¹².

Platelet-rich aggregates, such as leukocyte- and platelet-rich fibrin (L-PRF), have emerged as promising biological scaffolds due to their ability to release growth factors and support osteoprogenitor cell adhesion¹³. Derived from the patient's peripheral blood and obtained through different centrifugation protocols, these concentrates can release growth factors with high healing capacity^{14–17}. L-PRF, developed by Dohan et al., is a second-generation platelet concentrate produced through a single-step centrifugation process without anticoagulants, making it a low-cost and clinically accessible technique^{18–20}. The L-PRF membrane obtained exhibits a physiological structure that facilitates the healing process, serving as a scaffold for the adhesion of osteoprogenitor cells. Additionally, the platelets and leukocytes in the membrane ensure the continuous production and release of growth factors, making the technique cost-effective²¹, with applications that include hemostasis control in oral procedures^{22–24} and treatment of osteonecrosis of the jaws²⁵.

Bone tissue engineering focuses on enhancing bone regeneration and implant integration through biomaterials that promote osteoconduction (bone growth along a scaffold), osteoinduction (stimulation of progenitor cells), and osteogenesis (new bone formation from osteoprogenitor cells). The osseointegration process, which is fundamental for implant stability, is influenced by surface modifications and biological mediators that regulate bone deposition and remodeling.

Bone healing progresses through inflammatory, proliferative, and remodeling phases, where biomaterial-host interactions determine the quality of new bone formation. L-PRF serves as a bioactive scaffold, providing a sustained release of key growth factors (PDGF, TGF- β , VEGF) that enhance cell migration, adhesion, and osteogenic differentiation¹³. These properties align with bone tissue engineering principles, reinforcing L-PRF's role in early-stage bone regeneration.

Similarly, implant surface modifications, such as nanostructured hydroxyapatite coatings, enhance osteoconduction by mimicking bone mineral composition, improving biomaterial-host integration¹⁰. These coatings facilitate more efficient osseointegration, particularly in low-density bone environments.

This study hypothesizes that a titanium implant coated with nanostructured hydroxyapatite, combined with L-PRF, will promote superior osseointegration in over-instrumented bone sites, effectively simulating peri-implant defects. Thus, this study aims to compare peri-implant bone formation in implants with and without nanostructured hydroxyapatite coatings through histomorphometric analysis of bone-implant contact (BIC), bone area fraction occupancy (BAFo), and micro-CT evaluation.

Methods

Study design

The primary outcome measures of this study were bone-implant contact (BIC) and bone area fraction occupancy (BAFo), both assessed via histomorphometric analysis. The secondary outcome was the evaluation of bone microarchitecture using micro-computed tomography (μ CT), which included the analysis of bone volume fraction (BV/TV), trabecular thickness (Tb.Th), trabecular separation (Tb.Sp), and trabecular number (Tb.N). These parameters provided complementary quantitative insights into peri-implant bone response.

Model, animal maintenance, and ethical aspects

The authors selected the ovine model for this study due to its similarities with humans regarding weight, joint structure, bone tissue, and particularly its capacity for bone regeneration²⁶. Although the iliac crest is not a load-bearing site, it provides a well-controlled and standardized model for assessing early-stage osseointegration. The absence of functional loading minimizes confounding variables, such as occlusal forces, soft tissue interference, and variability in masticatory patterns, which can affect implant stability. Previous studies indicate that osseointegration parameters such as BIC and BAfo in the iliac crest show comparable trends to those observed in mandibular and maxillary models, making it a reliable experimental site²⁷. While functional loading is essential to long-term implant stability, future studies will incorporate mandibular or maxillary models to evaluate osseointegration under physiological forces.

This choice adheres to the 3Rs Program Guidelines (Reduction, Refinement, and Replacement) from the NC3Rs (Reporting Guidelines Working Group), which prioritize reducing the number of animals used in experimentation, minimizing pain and discomfort, and conducting tests on dental implant systems without requiring euthanasia²⁴. Additionally, the model is recommended by ISO/TS 22,911/2016 (Dentistry - Preclinical evaluation of dental implant systems - Animal test methods)²⁵ and is recognized as an experimental model for evaluating biomaterials in bone sites^{26,27}.

Five healthy female Santa Inês sheep with skeletal maturity (minimum age of 2 years) and weighing between 40 and 45 kg were selected for this study. The animals selected were skeletally mature, free from systemic diseases, and without orthopedic or metabolic conditions that could affect bone remodeling. No exclusion criteria were applied beyond ensuring overall health. They were housed in suspended pens at the Goat and Sheep Sector

of the UFF Experimental Farm, receiving a diet of chopped grass and corn silage, supplemented with 12% crude protein (CP) feed and mineral salt, with ad libitum access to filtered water throughout the experiment. Animal supervision, as well as dietary and preoperative fasting management, was carried out by two experienced veterinarians.

The sheep were transferred from the breeding facility to the research center two weeks before surgery, ensuring adequate acclimatization and minimizing preoperative stress. The fasting protocol was established: solids were restricted to half rations 48 h before surgery, transitioning to zero diet 24 h before surgery, and liquids were held 12 h before surgery.

All experimental protocols were approved by the Ethics Committee for Animal Use of Fluminense Federal University (CEUA-UFF# 1172100123). The animal experiments occurred during the first half of 2023. All methods were carried out in accordance with relevant guidelines and regulations. All methods were reported in accordance with Animal Research: Reporting of In vivo Experiments (ARRIVE)²⁸ and Planning Research and Experimental Procedures on Animals: Recommendations for Excellence (PREPARE)²⁹ guidelines where appropriate. Euthanasia of the animals was not necessary because the bone samples containing the implants were removed from the iliac crest without compromising any vital function of the animals. The animals were kept alive and returned to the reproduction department of the Veterinary school of Fluminense Federal University experimental farm. The source of these animals for the study was the animal reproduction department of the veterinary school of Fluminense Federal University.

Sample size calculation

The sample size calculation was performed using the Sealed Envelope platform (<https://www.sealedenvelope.com/power/continuous-superiority/>). Data from Sartoretto³⁰ et al. (2020) were used, where the mean bone formation area (primary variable) was 65.53%, with a standard deviation of 6.23% for the control group. Using a 5% significance level, a statistical power (1- β) of 90%, and considering a 20% increase in the experimental group, the calculation determined that five implants per group were necessary for statistical reliability.

Implants, surface characteristics, and biomaterials

A total of 20 titanium dental implants were used, with dimensions of 3.5 mm in diameter and 10 mm in length, divided into two experimental groups: the HAnano group (Epikut Plus[®]; SIN- Implant System, São Paulo, Brazil), with a nanohydroxyapatite coating, and the DAA group (Epikut[®]; SIN- Implant System, São Paulo, Brazil), with a surface treated by double acid etching. For the groups subjected to peri-implant grafting, L-PRF (Leukocyte and Platelet Rich Fibrin) was used, an autogenous material obtained from the centrifugation of the sheep's peripheral blood.

Anesthesia procedures

All procedures that could induce anxiety and pain were performed under general anesthesia and conducted by an experienced veterinary anesthesiologist. Before the procedure, the animals underwent a food and water deprivation protocol following UniPECO guidelines and were weighed on a precision digital scale (Urano UR 10000 Light Platform Scale).

For general anesthesia, the animals received pre-anesthetic medication, including Acepromazine 0.05 mg/kg (Acepran[®]-Vetnil, Louveira, São Paulo, Brazil) and Diazepam 0.2 mg/kg (Diazepam-Teuto[®], Anápolis, Goiás, Brazil) administered intravenously, as well as Morphine 0.4 mg/kg administered intramuscularly (Dimorf[®] - Cristália, Itapira, São Paulo, Brazil). After 20 min, the cephalic vein was cannulated for fluid therapy with Ringer's lactate solution infused at a 5 ml/kg/h rate. Anesthetic induction was administered to effect using Propofol 4 mg/kg (Baxter Hospitalar LTDA, São Paulo, Brazil).

The animals were then intubated via the orotracheal route using a tube compatible with their weight, and anesthesia was maintained with Isoflurane (Isoflurane[®] - Cristália, Itapira, São Paulo, Brazil), adjusted according to autonomic pain responses. After a two-hour observation period for anesthetic recovery, the animals were returned to their pens with free access to feed and water.

Preparation of L-PRF

Venous blood was drawn using 21G needles (BD Brazil) from the five sheep. The collected blood was immediately transferred to two 9 ml red cap tubes (BD, São Paulo, Brazil) without anticoagulants (BD Vacutainer[®], Becton Serum Blood Collection Tubes, Dickinson & Company, Franklin Lakes, NJ, USA) at room temperature, 22°C, with centrifugation at 2700 rpm for 12 min (~708 g) using a fixed angle/vertical centrifuge (IntraSpin[™], Biohorizons[®], Birmingham, AL, USA). This centrifugation protocol considers the g-force value referenced to the bottom of the centrifuge tubes (RCF-max)³¹. After clot formation, the solid L-PRF was removed from the tubes and dehydrated on a perforated grid within a specialized case, producing L-PRF membranes. These membranes were immediately implanted into the peri-implant spaces of the designated experimental groups. No additional storage was performed to preserve the biological activity of growth factors released by L-PRF.

Surgical procedures

The surgical procedures were carried out in two stages:

Stage 1 – Implant Placement.

After antiseptic of the surgical area with 0.5% alcoholic chlorhexidine (Riohex[®] 0.5%, São José do Rio Preto, SP, Brazil), sterilized surgical drapes were positioned to isolate and define the operative areas. An incision was made on the skin using a No. 3 scalpel handle (Bard Parker[®], São Paulo, SP, Brazil) and a No. 15 blade (Solidor[®] - Lamedid, Osasco, SP, Brazil). Tissue dissection was performed until the skeletal plane was exposed.

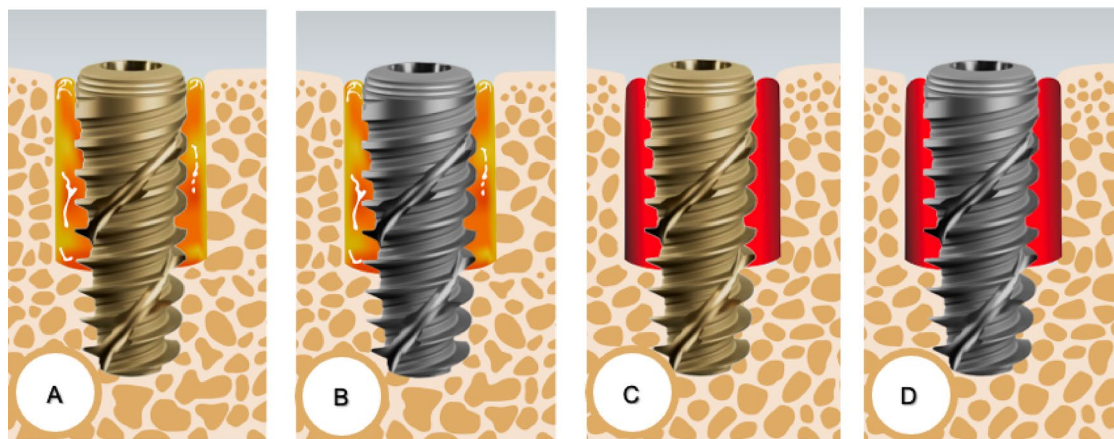


Fig. 1. Overview of implant placement and peri-implant biomaterial distribution across experimental groups ($n = 5$ per group, total = 20 implants): (A) Epikut Plus* (HANano) in an L-PRF-filled site (Group 1); (B) Epikut* (DAA) in an L-PRF-filled site (Group 2); (C) Epikut Plus* (HANano) in a blood-filled site (Group 3); (D) Epikut* (DAA) in a blood-filled site (Group 4). This figure illustrates implant surface variations and peri-implant grafting conditions. The image was kindly provided by Dr. Helder Valiense and created using CorelDRAW, version 21.

Experimental Groups ($n = 5$ /group)	Surface treatment	Peri-implant grafts
Group 1	HANano	L-PRF
Group 2	DAA	L-PRF
Group 3	HANano	Blood
Group 4	DAA	Blood

Table 1. Distribution of experimental groups based on implant surfaces and grafting with L-PRF or blood filling.

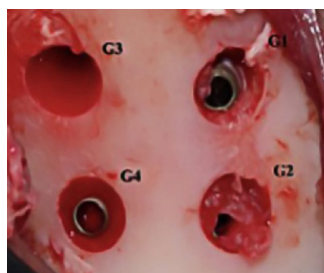


Fig. 2. Surgical procedure for implant placement in the iliac crest. The image illustrates incision, bone exposure, and implant positioning, following the experimental protocol for peri-implant biomaterial placement.

Immediately following tissue dissection, 6 mm diameter and 4 mm depth bone trephinations were performed using a trephine drill, and the bone blocks were removed. Biomaterials were implanted according to the experimental groups (Fig. 1). This figure illustrates the differentiation between the type of implant and the graft material used in each group, establishing a basis for subsequent comparative analyses. Subsequently, one implant from each experimental group was placed in every sheep, totaling four implants per animal, following the manufacturer's guidelines and the descriptions in Table 1.

The region containing the implants was sutured using 3.0 Mononylon thread to achieve primary skin closure. The animals were monitored at the farm, and the veterinarian administered postoperative medication as recommended.

Figure 2 depicts the surgical sites in the iliac crest where implants were placed with or without L-PRF grafting, providing a clear overview of implant location and immediate postoperative appearance.

Four trephinations were performed to create the peri-implant gap, and the sites were filled with biomaterials according to the experimental groups. After filling, the implants were placed using the drill sequence

recommended by the manufacturer, at low rotation (1200 RPM) and intermittently, with abundant irrigation using 0.9% sodium chloride solution (Darrow Laboratórios S.A., Rio de Janeiro, RJ, Brazil) to prevent tissue necrosis from overheating. Implant placement was conducted with a contra-angle attached to a surgical electric micromotor (Driller[®], BPM-600 Plus, São Paulo, SP, Brazil) at 14 RPM, with a minimum pre-set torque of 50 Ncm. This approach facilitated the creation of a 5 mm overprepared site, with the 10 mm implant apically locked.

Implant placement was alternated in the mesiodistal positions for each group, with the first position chosen randomly. This alternation ensured that the same group of implants was not consistently placed in the same location in all sheep. After placing the four implants, the skin was closed with interrupted simple sutures using 3.0 Nylon thread (Johnson & Johnson[®], Rio de Janeiro, RJ, Brazil).

Stage 2 – Obtaining bone blocks

Eight weeks after implant placement, the animals underwent the same general anesthesia protocol. A standard surgical procedure was performed to collect bone samples containing the implant and adjacent bone for subsequent histological and histomorphometric analysis.

Eight weeks after surgery, an 8 mm trephine drill (SIN-Implant System) was used to collect bone blocks containing the implants and peri-implant tissue for histological processing. After making an incision and exposing the skeletal plane (Fig. 3A), the trephine drill was used to mark the site (Fig. 3B) and surgically extract the bone block along the implant's longitudinal axis (Fig. 3C and D). Immediately after collection, the samples were fixed in 3.7% buffered formaldehyde. All animals remained alive after the procedure and were returned to the farm following recovery.

Postoperative pain control

All animals received antibiotic therapy for pain management and infection prevention via intramuscular injection of Oxytetracycline at 0.1 ml/kg (Terramicina[®] – Pfizer, São Paulo, SP, Brazil), administered every 48 h for 3 days. Analgesia was maintained with Tramadol 4 mg/kg (Tramal[®] – Pfizer, São Paulo, SP, Brazil), and anti-inflammatory control was achieved with Meloxicam 0.5 mg/kg (Meloxivet[®] – Duprat, Rio de Janeiro, RJ, Brazil), both administered intramuscularly for 5 days.

Laboratory processing of samples for resin embedding

The recovered blocks were stored in plastic containers with 3.7% buffered formaldehyde for 48 h. After fixation, the samples were washed in running water for 24 h and gradually dehydrated in increasing ethanol concentrations (60%, 80%, 96%, and 100%), with exchanges every 3 days.

After dehydration, the samples were infiltrated with Technovit resin (7200 VLC, Kulzer Heraeus GmbH & Co., Wehrheim, Germany), with successive resin substitutions at increasing concentrations (30%, 50%, 70%, and 100%) every 3 days. The samples were then placed in plastic bases and covered with Technovit resin for embedding and block formation, using a light source for polymerization.

The blocks containing the implant and peri-implant tissue were glued onto pre-sanded and cleaned plastic slides and adjusted in the EXAKT 300 CP series system (Apparatebau, Germany) for cuts in the apical-coronal direction. The cut along the central axis of the implant exposed its internal surface. This section was glued onto

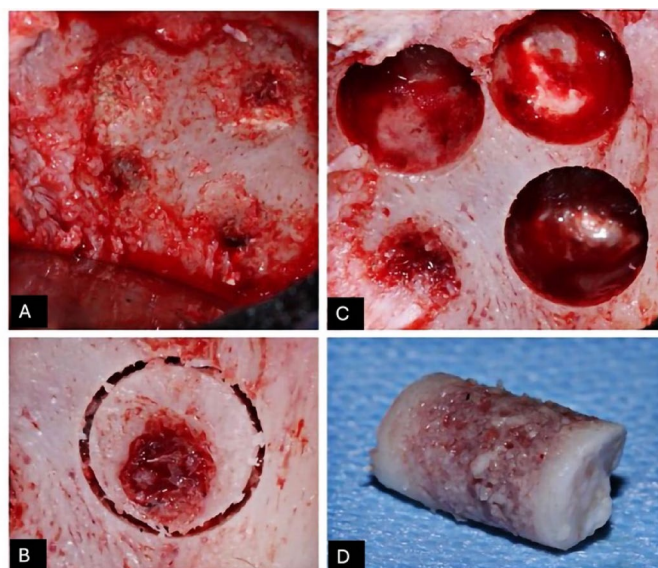


Fig. 3. Sample collection process for histological and histomorphometric analysis, performed eight weeks after implantation. (A) Iliac crest showing bone repair at the implant site; (B) Marking of the trephination site for bone block extraction; (C) Bone blocks containing implants retrieved for histological evaluation; (D) Bone block with implant and peri-implant tissue, prepared for analysis.

a second slide to allow the reduction of the fragment to the final thickness of approximately 70 μm , using a polishing protocol with abrasive papers of 800, 1000, 1200, and 2400 grit (EXAKT 310 CP series, Apparatebau, Germany), under constant water irrigation.

The resulting histological sections were stained with Toluidine Blue and Basic Fuchsin, covered with glass coverslips fixed with Entellan[®] (Merck[®], Darmstadt, Germany).

Histological descriptive evaluation

The slides were analyzed under a light field microscope (OLYMPUS BX43, Tokyo, Japan), and images were captured using the CELLSSENS[®] acquisition software (Olympus Corporation, Tokyo, Japan).

Before positioning the slides on the microscope stage, each was carefully cleaned with tissue to remove impurities. The microscope illumination was kept constant throughout all image capture sessions, with the tungsten lamp potentiometer set to the 12 o'clock position.

Photomicrographs were captured at magnifications of 10x and 20x, using continuous field scanning to visualize the entire implant area and adjacent bone. For more detailed analysis, 20x magnification images were obtained, focusing on the tissues filling the spaces between the threads and the implant/bone interface.

Histomorphometric evaluation

Histomorphometric analysis was performed using Image Pro Plus software to quantify BIC (%) and BAfo (%), representing the extent of new bone formation at the implant interface. Photomicrographs were captured at 10x magnification in sequential, non-overlapping fields for each slide obtained from histological processing, covering the entire implant surface. These photomicrographs were reconstructed to generate a complete image of the implant area and adjacent bone. After reconstruction, a rectangular area of interest (36 μm long and 10 μm wide) was delimited, extending vertically from the first thread of the implant to the beginning of the fourth thread and horizontally along the longitudinal axis of the implant body (Fig. 4A).

The area of interest was then cropped (Fig. 4B) and transferred to the Image Pro Plus software, where a grid was overlaid with 18 vertical lines (parallel to the implant axis) and 62 horizontal lines (perpendicular to the implant axis), all equidistant (Fig. 4C). The intersections of these lines (a total of 1116 points) were classified according to the variables of this study: newly formed bone, biomaterial, or connective tissue. This enables the calculation of the bone area fraction (BAfo) (Fig. 5).

The bone-implant contact (BIC) value was obtained by counting the number of horizontal lines coinciding with the implant surface where direct contact with the bone was present. The results of the BAfo and BIC analyses were expressed as percentages, calculated from the total number of intersections (BAfo) or valid lines (BIC). Points on the titanium and "white" areas caused by surgical or histological artifacts were excluded from the analyses.

Microtomographic evaluation

Due to their low linear attenuation coefficients, titanium implants are ideal for X-ray microtomography (μCT) investigations. μCT is a non-destructive technique that generates images of specific material cross-sections from planar projections, allowing quantitative and qualitative trabecular bone microstructure analysis. Due to its high resolution, this technique is particularly suited for examining bone morphology, offering advantages over conventional methods.

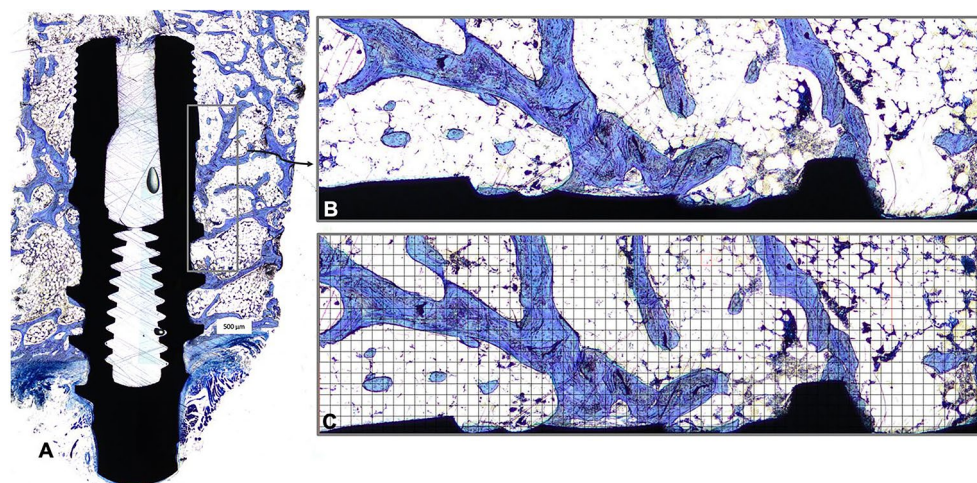


Fig. 4. Histomorphometric method for evaluating bone-implant contact (BIC) and bone area fraction occupancy (BAfo). (A) Histological reconstruction of the implant and peri-implant tissues; (B) Delineation of the area of interest (36 $\mu\text{m} \times 10 \mu\text{m}$), spanning the first to fourth implant threads; (C) Grid overlay with 18 vertical and 62 horizontal equidistant lines for quantitative analysis. Staining: Toluidine blue. Scale bar: 500 μm . This method provides a detailed assessment of the implant-bone interface.

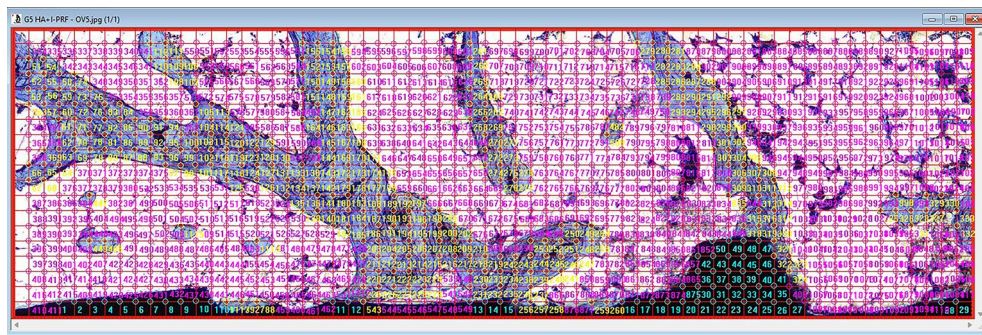


Fig. 5. Image ProPlus software interface is used to classify grid intersections into new bone, biomaterial, or connective tissue, enabling BAfo quantification. The image illustrates the software's role in data processing and its application in evaluating peri-implant material integration.

μ CT is particularly effective for assessing trabecular bone organization in the peri-implant region. Following image acquisition, microtomographic parameters were analyzed to characterize bone structure quantitatively and qualitatively. This study evaluated bone microarchitecture using bone volume fraction (BV/TV), trabecular thickness (Tb.Th), trabecular separation (Tb.Sp), and trabecular number (Tb.N) providing a comprehensive assessment of peri-implant bone quality and structure.

Five samples were subjected to micro-computed tomography (μ CT) using a SkyScan 1275 device (Bruker) at the Experimental Endodontics Laboratory (LEE) of UFF. The scanning parameters included 65 kV, 80 mA, and an isotropic pixel size of 8.5 μ m (0.085 mm), following the Guidelines for the Acquisition and Evaluation of Bone Microstructure in Rodents^{32–34}.

For the tomographic slices, images of all samples were repositioned along the longitudinal axis using DataView software (Bruker microCT), ensuring complete visualization of the samples. The sagittal slice images were then exported to CTAn software (Bruker), where a 3D Region of Interest (ROI) was applied around the bone formation area surrounding the implants for quantitative morphometric analysis.

Statistical analysis

Statistical analyses were conducted using Prism software (v. 10, GraphPad R). Descriptive statistics included the calculation of mean, median, standard deviation, variance, and 95% confidence intervals. Data normality was assessed using the Shapiro-Wilk test. Variance homogeneity was verified with Levene's or Brown-Forsythe's test when normality was not met. Outliers were identified and removed using a 1% threshold using the ROUT method.

For group comparisons, Brown-Forsythe analysis of variance (ANOVA) and Welch's ANOVA were used for primary outcomes (BIC and BAfo). Since μ CT parameters (BV/TV, Tb.Th, Tb.Sp, Tb.N) did not meet normality assumptions, the Kruskal-Wallis test was applied for these variables. Additionally, Brown-Forsythe and Welch ANOVA were used when variance heterogeneity was detected, followed by Dunnett's T3 post-test for multiple comparisons. Statistical significance was set at $p < 0.05$.

Results

Clinical evaluation of animals

All animals tolerated the trans and postoperative period well, without signs of infection or necrosis. The anesthetic and surgical procedures were uneventful; all five sheep recovered quickly and were allowed to roam shortly after surgery. During the 8-week postoperative period, all animals received food and water regularly, without superficial or deep infections, and sheep showed an average weight gain of 4%.

Descriptive histological evaluation

Experimental groups 1, 2, 3, and 4 showed similar histological characteristics, with areas of bone-implant contact and small amounts of newly formed bone trabeculae (Fig. 6).

Histomorphometric results

The histomorphometric analysis of the implant-bone tissue interface (BIC) and connective tissue (CT) showed normal distribution, confirmed by the Shapiro-Wilk test ($p > 0.05$), homogeneity of variances ($p > 0.05$, Levene's test) and Q-Q probability plot. Brown-Forsythe and Welch ANOVA were used when variance heterogeneity was detected, followed by Dunnett's T3 post-test for multiple comparisons. No statistically significant differences were identified among groups ($p > 0.05$). On average, bone-implant contact ranged from 44% (HANano + L-PRF) to 63% (DAA + L-PRF), while the surface covered with connective tissue ranged from 37 to 56% in the same experimental groups. In the peri-implant region, bone volume density varied between 44 and 63%, with the HANano group associated with L-PRF showing greater dispersion in the data (Fig. 7A). No significant differences were observed between groups regarding connective tissue volume density, which ranged from 37 to 56% (Fig. 7B).

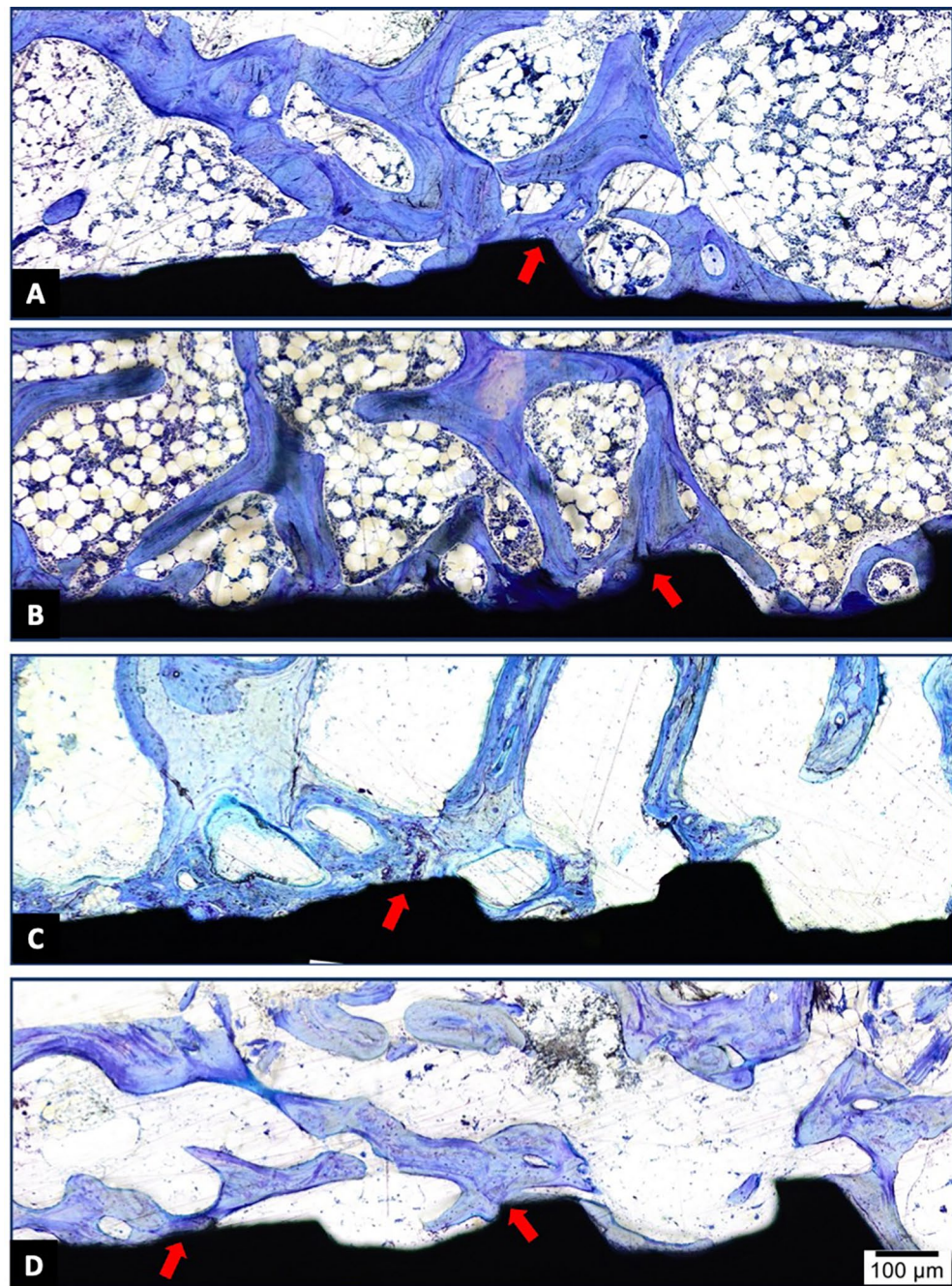


Fig. 6. Photomicrographs of the peri-implant region eight weeks post-implantation. (A) HANano + L-PRF, (B) DAA + L-PRF, (C) HANano + Blood (Sham), (D) DAA + Blood (Sham Group). Red arrows highlight bone-implant contact (BIC) areas. Staining: Toluidine blue. Magnification: 20x; Scale bar: 100 μm . The images show newly formed bone trabeculae across different treatment groups.

The histomorphometric analysis of the bone area fraction occupancy (BAFo) and connective tissue (CT) showed normal distribution, confirmed by the Shapiro-Wilk test ($p > 0.05$), homogeneity of variances ($p > 0.05$, Levene's test) and Q-Q probability plot. Brown-Forsythe and Welch ANOVA were used when variance heterogeneity was detected, followed by Dunnett's T3 post-test for multiple comparisons. No statistically significant differences were identified among groups ($p > 0.05$). In the peri-implant region, bone volume density varied between 26 and 39% (Fig. 8A). No significant differences were observed between groups regarding connective tissue volume density, which ranged from 48 to 68% (Fig. 8B).

Microtomography results

Microtomographic analyses were performed using three strategies, considering the images' bone tissue and biomaterial separately. Quantification was conducted to include the combined signal from bone and biomaterial

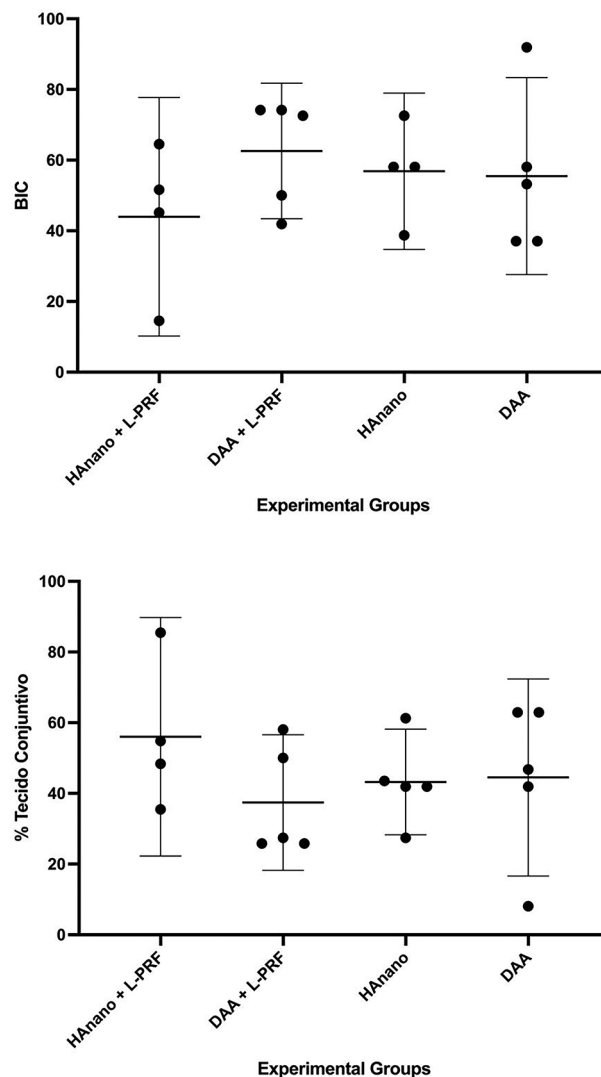


Fig. 7. Bone-implant contact (BIC) and connective tissue (TC) percentages in experimental groups (HAnano + L-PRF, DAA + L-PRF, HAnano Sham, DAA Sham). Histomorphometric analysis showed no significant differences (Brown-Forsythe and Welch ANOVA, $p > 0.05$). BIC ranged from 44–63%, while connective tissue surface ranged from 37–56%. Data are presented as mean \pm 95% confidence intervals.

and individual analyses of bone and biomaterial alone. The results indicated no significant differences in the percentage of bone volume and the percentage of biomaterial volume when analyzed in isolation, as shown in Fig. 9.

The microtomographic analysis of the structural characteristics of the peri-implant bone revealed no statistically significant differences between the experimental groups DAA SHAM, HAnano SHAM, HAnano LPRF, and DAA LPRF for any of the variables analyzed (Fig. 10). The Bone Volume Percentage (BV/TV, A) indicated that the treatments did not influence the amount of bone tissue about the total volume, while the Bone Surface/Volume Ratio (BS/BV, B) demonstrated that the complexity and compaction of the bone structure were similar in all groups. Likewise, the Bone Surface Density (BS/TV, C) remained comparable between the groups, with no impact from the treatments applied, and the Surface Intersection Percentage (iS/TS, D) did not present significant variations, demonstrating that the interconnectivity and structural integrity of the bone tissue were consistent. The results, evaluated by the Kruskal-Wallis test and Dunn's post-test ($p < 0.05$), suggest that the treatments applied did not produce detectable changes in the structural characteristics of the peri-implant bone.

Discussion

This study aimed to evaluate the effectiveness of nanostructured hydroxyapatite coating (HAnano) and leukocyte- and platelet-rich fibrin (L-PRF) in the osseointegration of dental implants installed in over-instrumented sites in sheep, using histological, histomorphometric, and microtomographic analyses. The histomorphometric findings (BIC and BAFO) and micro-CT parameters comprehensively evaluated peri-implant bone response, allowing us to assess the effect of surface treatment and L-PRF under controlled conditions. Our findings indicate that

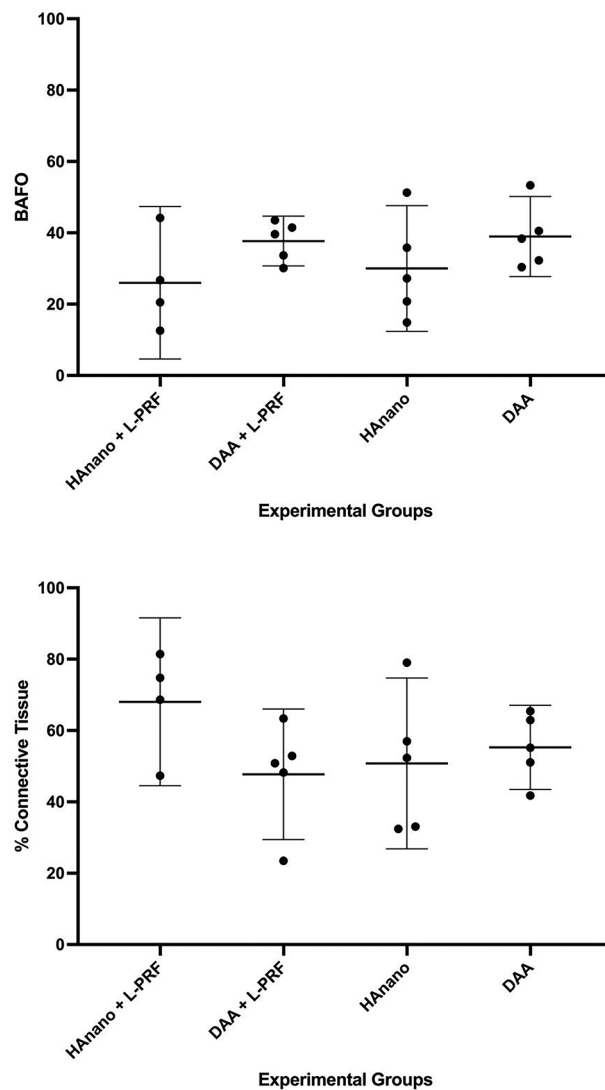


Fig. 8. Comparative analysis of bone volume density (BAFo) and connective tissue (TC) percentages in the peri-implant region across experimental groups. No significant differences were observed (Brown-Forsythe and Welch ANOVA, $p > 0.05$). BAFO ranged from 26–39%, while connective tissue density varied between 48% and 68%. Data are presented as mean \pm 95% confidence intervals.

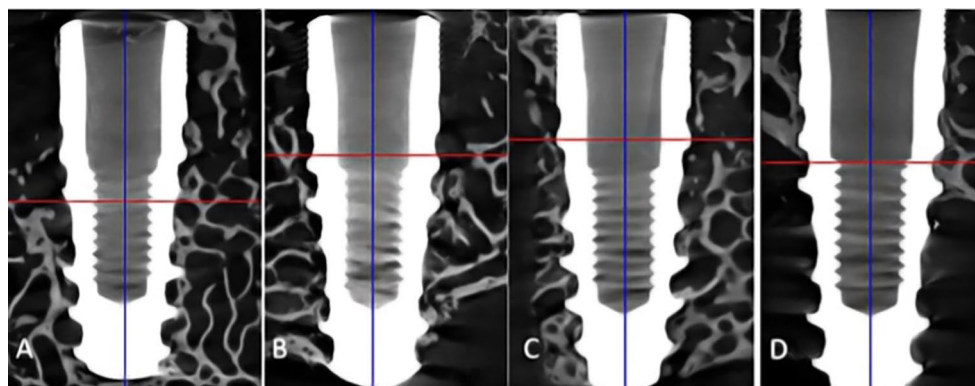


Fig. 9. Microtomographic images of the experimental groups. (A) HAnano + Blood (Sham); (B) HAnano + L-PRF; (C) DAA + Blood (Sham) and (D) DAA + L-PRF.

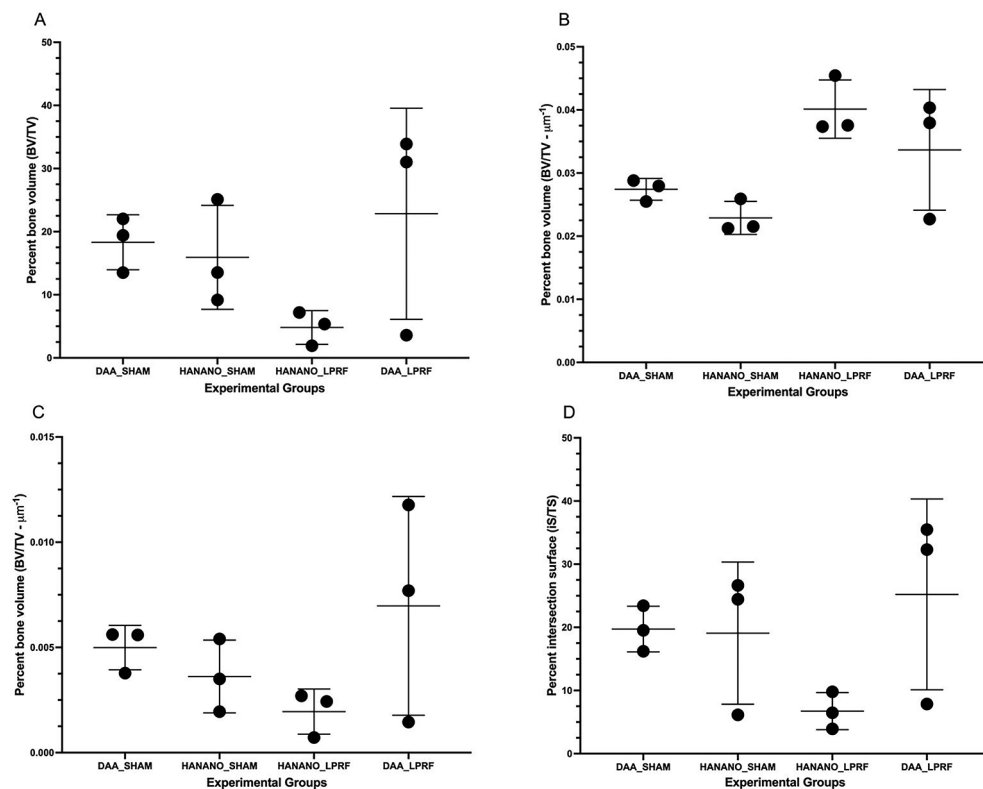


Fig. 10. Microtomographic analysis of bone structures across experimental groups (DAA_SHAM, HANANO_SHAM, HANANO_LPRF, and DAA_LPRF), evaluating bone volume percentage (BV/TV), bone surface-to-volume ratio (BS/BV), bone surface density (BS/TV), and surface intersection percentage (iS/TS). Data are presented as mean \pm standard deviation. Statistical analysis was performed using the Kruskal-Wallis test followed by Dunn's post-test, revealing no significant differences between groups ($p > 0.05$; $n = 3$).

all four experimental groups, combining HANano, DAA, L-PRF, and blood, exhibited similar bone-to-implant contact (BIC) and bone area fraction occupancy (BAFo), with no significant differences.

Albrektsson highlights that studies involving the bone-implant interface aim to promote osteoinduction, osteoconduction, and osseointegration to reduce the postoperative waiting time before applying functional occlusal loading¹¹. In line with this objective, we chose to use adult sheep, as in Sartoretto et al., to provide an anatomical model with body weight and bone dimensions like those of humans³⁶. These characteristics allow for a more accurate simulation of large-scale prosthetic implantation²⁶. Furthermore, the sheep model allows the trephination of a bone block containing the implant and the grafted material in the peri-implant region for histological, histomorphometric, and microtomographic analysis.

L-PRF, an autogenous biomaterial that is easy to prepare, proved effective, releasing large amounts of growth factors such as TGF- β 1, VEGF, and PDGF-AB for up to seven days^{37–39}. These factors play crucial roles in accelerating soft and hard tissue repair, as noted by Ondur et al., justifying its use in socket preservation, periodontal surgery, sinus lift, and bone reconstruction⁴⁰. Yurttutan et al. observed rapid osseointegration in implants with hydroxyapatite after one month, although they noted a decrease after three months³⁵.

Studies by Lyris et al.⁴¹, Benalcázar et al.⁴², and Almeida et al.⁴³ support the notion that L-PRF contributes to the secondary stability of implants by promoting initial bone formation in dental implants. Sartoretto et al.³⁰, who reported significant increases in BIC and BAFo values at 14 and 28 days on HANano and DAA surfaces, reinforce this observation. These findings indicate that nanostructured surfaces and L-PRF play synergistic roles in improving osseointegration.

The results of this study, along with those of Almeida et al.⁴³ and Sartoretto et al.³⁰, suggest that HANano and DAA surfaces promote osseointegration, with HANano demonstrating superior performance in some bone regeneration metrics. Hydroxyapatite is widely recognized for its biocompatibility, low biodegradability, bone affinity, and osteoconductivity, making it an ideal choice for implants⁴³. However, the BIC and BAFo values obtained, although significant, represent specific time points and may not fully capture the dynamic process of osseointegration, as highlighted by Almeida et al.⁴³ and Sartoretto et al.³⁰. Subsequent studies, including long-term evaluations, may provide a more comprehensive view of the development of the bone-implant interface over time.

Bone healing chambers (BHCs) have been explored to enhance bone remodeling in low-density bone environments. Recent studies suggest that osseodensification enhances early-stage bone healing by creating bone healing chambers (BHCs) around the implant, facilitating osteoconduction while maintaining primary stability⁴⁴.

Similarly, the present study observed bone remodeling within a controlled peri-implant space, supporting the role of healing chambers in osseointegration. Combining an optimized implant site preparation and bioactive implant surfaces, such as nanostructured hydroxyapatite coatings, may further enhance osseointegration in low-density bone models, such as the iliac crest.

The micro-CT analysis revealed no significant differences between experimental groups, suggesting that neither the implant surface treatment nor the presence of L-PRF had a measurable effect on trabecular microarchitecture within the eight-week evaluation period. This result is in line with previous studies indicating that the primary effects of L-PRF on bone healing occur in the early stages, predominantly through the release of growth factors within the first weeks post-implantation. Since bone remodeling is a continuous process, more extended observation periods might be required to assess potential differences in bone microarchitecture that were not detectable within the eight-week timeframe. Furthermore, variations in species-specific bone metabolism may also influence the outcomes, as sheep exhibit distinct bone remodeling patterns compared to humans²⁷.

Although HAnano and L-PRF have shown benefits in osseointegration, this study underscores the importance of standardizing measurements and surface evaluations to maximize results. Wennerberg & Albrektsson² emphasized that the lack of standardization in surface measurements complicates comparisons between studies, as surfaces described as “rough” in one study may be considered “smooth” in another. To address this limitation, stricter standardization of measurement techniques is recommended to ensure comparability and precision of results.

Additionally, growth factor release kinetics and osteoblastic behavior may vary between species. Luginbuehl et al.⁴⁵ demonstrated that the release of IGF-I in sheep occurs differently, and it is essential for optimal osteogenesis. Al-Musawi et al.⁴⁶ identified specific differences in the expression and activity of BMP-15, which may affect bone repair in a species-specific manner.

Despite L-PRF's proven advantages over the past twenty years⁴⁷, its full impact on healing and bone repair remains an area of investigation. Future studies should focus on the longitudinal analysis of the bone-implant interface behavior, evaluating the effects of nanostructured surfaces and L-PRF over longer periods. These studies could include comparisons between different animal models and the analysis of additional microtomographic parameters to deepen the understanding of the interaction between biomaterials and bone.

This study presents several strengths that enhance the reliability and translational value of the findings. First, using sheep as a large-animal model provides a well-established and biologically relevant platform for studying implant osseointegration, as their bone structure and remodeling dynamics closely resemble those of humans²⁷. Additionally, the study design ensured standardization, with each animal receiving implants from all experimental groups, reducing inter-individual variability and allowing for a robust intra-subject comparison. Furthermore, micro-computed tomography (μ CT) and histomorphometric analyses provided complementary quantitative and qualitative data, comprehensively evaluating peri-implant bone response. HAnano and DAA surface-treated implants further contribute to the growing body of research on the impact of surface modifications on osseointegration.

Despite its strengths, the study has some limitations. The absence of functional loading in the iliac crest model is a key constraint, as it does not fully replicate the masticatory forces experienced by implants in clinical settings. Additionally, species-specific differences in bone metabolism, osteoblastic activity, and growth factor release kinetics may influence osseointegration outcomes. Previous studies have shown that growth factor expression, particularly in response to biomaterials, varies across species, impacting bone regeneration rates and implant integration⁴⁶. Therefore, while the findings of this study provide valuable insights, further research incorporating comparative studies in human-like load-bearing models is warranted to enhance translational relevance.

However, this model was selected to minimize confounding variables and allow for a controlled assessment of early osseointegration. Future studies will incorporate mandibular or maxillary placement models to evaluate implant stability under functional loading conditions. Another limitation is the lack of long-term evaluation of L-PRF effects, as this study focused on early osseointegration markers within eight weeks. Given that L-PRF exerts its biological effects predominantly in the initial weeks, further investigations with extended follow-up periods are needed to assess its influence on bone remodeling and implant stability. Additionally, differences in vascularity between the iliac crest and the jawbones (mandible and maxilla) may affect bone healing dynamics, necessitating cautious extrapolation of results to clinical scenarios. Future studies comparing vascularized vs. non-vascularized implantation sites will provide further insights into the influence of bone perfusion on osseointegration outcomes.

This study evaluated the impact of nanostructured hydroxyapatite-coated implant surfaces and peri-implant grafting with leukocyte- and platelet-rich fibrin (L-PRF) on osseointegration in over-drilled sites using an ovine model. Histomorphometric and microtomographic analyses revealed that HAnano and double acid-etched (DAA) implant surfaces successfully promoted osseointegration in low-density bone conditions. However, no statistically significant differences were observed between the experimental groups, indicating that neither the implant surface treatment nor the presence of L-PRF significantly enhanced bone-implant contact (BIC) or bone area fraction occupancy (BAFo) within the 8-week study period. Despite L-PRF's known bioactive properties and potential to enhance early-stage bone healing, its effect on long-term osseointegration remains uncertain and requires further investigation. Additionally, while the iliac crest model provides a controlled environment for analyzing bone healing, its biomechanical conditions differ from load-bearing sites such as the mandible, limiting the direct extrapolation of results to clinical scenarios. Future studies should explore longer evaluation periods to assess the extended effects of L-PRF on bone regeneration and implant stability. Moreover, comparative analyses in load-bearing anatomical sites, such as the jaw, could provide a more clinically relevant perspective on the interaction between implant surface modifications and biologically active biomaterials.

Data availability

The datasets used and/or analyzed during the current study available from the corresponding author on reasonable request.

Received: 4 December 2024; Accepted: 9 April 2025

Published online: 28 April 2025

References

- Klein, M. O. et al. Al-Nawas, B. Submicron scale-structured hydrophilic titanium surfaces promote early osteogenic gene response for cell adhesion and cell differentiation. *Clin. Implant Dent. Relat. Res.* **15**, 166–175 (2013).
- Wennerberg, A. & Albrektsson, T. Effects of titanium surface topography on bone integration: a systematic review. *Clin. Oral Implants. Res.* **20**, 172–184 (2009).
- Elias, C. N. & Meirelles, L. Improving osseointegration of dental implants. *Expert Rev. Med. Dev.* **7**, 241–256 (2010).
- Sartoretto, S. C. et al. Early osseointegration driven by the surface chemistry and wettability of dental implants. *J. Appl. Oral Sci.* **23** (3), 279–287 (2015).
- Sartoretto, S. C. et al. Hydrophilic surface of Ti6Al4V-ELI alloy improves the early bone apposition of sheep tibia. *Clin. Oral Implant Res.* **28** (8), 893–901 (2016).
- AlFarraj Aldosari, A. et al. The influence of implant geometry and surface composition on bone response. *Clin. Oral Impl Res.* **00**, 1–6 (2013).
- Vasak, C. et al. Early bone apposition to hydrophilic and hydrophobic titanium implant surfaces: a histologic and histomorphometric study in minipigs. *Clin. Oral Impl Res.* **25**, 1378–1385 (2014).
- Bordea, I. R. et al. Todea DA: Nano-hydroxyapatite use in dentistry: a systematic review. *Drug Metab. Rev.* <https://doi.org/10.1080/03602532.2020.1758713> (2020).
- Ong, J. L. & Chan, D. C. N. A review of hydroxyapatite and its use as a coating in dental implants. *Crit. Reviews TM Biomedical Eng.* **45** (1–6), 291–319 (2017).
- Wang, X., Wan, C., Feng, X., Zhao, F. & Wang, H. Vivo and in vitro analyses of Titanium-Hydroxyapatite functionally graded material for dental implants. *BioMed. Res. Int. Biomed. Res. Int. Apr.* **30**, 20218859945. <https://doi.org/10.1155/2021/8859945> (2021).
- Albrektsson, T. & Johansson, C. Osteoinduction, osteoconduction and osseointegration. *Eur. Spine J.* **10** (suppl 2), S596–S101 (2001).
- Lang, N. P. et al. Early osseointegration to hydrophilic and hydrophobic implant surfaces in humans. *Clin. Oral Impl Res.* **22**, 349–356 (2011).
- Dohan Ehrenfest, D. M. et al. Platelet-rich fibrin (PRF): a second-generation platelet concentrate. Part II: leucocyte activation: a new feature for platelet concentrates? *Oral Surg. Oral Med. Oral Pathol. Oral Radiol. Endodontology.* **101** (3), 45–50 (2006).
- Dohan Ehrenfest, D. M. et al. Classification of platelet concentrates (Platelet-Rich Plasma-PRP, Platelet-Rich Fibrin-PRF) for topical and infiltrative use in orthopedic and sports medicine: current consensus, clinical implications, and perspectives. *Muscles Ligaments Tendons J.* **4** (1), 3–9 (2014).
- Dohan Ehrenfest, D. M. et al. Platelet-rich fibrin (PRF): A second-generation platelet concentrate. Part III: leucocyte activation: a new feature for platelet concentrates? *Oral Surg. Oral Med. Oral Pathol. Oral Radiol. Endod.* **101**(3), e51–5 (2006).
- Dohan Ehrenfest, D. M. et al. Platelet-rich fibrin (PRF): a second-generation platelet concentrate. Part I: technological concepts and evolution. *Oral Surg. Oral Med. Oral Pathol. Oral Radiol. Endod.* **101**(3), e37–44 (2006).
- Dohan Ehrenfest, D. M. et al. In search of a consensus terminology in the field of platelet concentrates for surgical use: platelet-Rich plasma (PRP), platelet-Rich fibrin (PRF), fibrin gel polymerization and leukocytes. *Curr. Pharm. Biotechnology* **12**, 1131–1137 (2012).
- Dohan Ehrenfest, D. M. & Rasmusson, L. And Albrektsson classification of platelet concentrates: from pure platelet-rich plasma (P-PRP) to leucocyte- and platelet-rich fibrin (L-PRF). *Cell. Press. - Trends Biotechnol.* **27** (3), 158–167. <https://doi.org/10.1016/j.tibtech.2008.11.009> (2009).
- de Mourão, C. F. The use of platelet-rich fibrin as a hemostatic material in oral soft tissues. *Oral Maxillofac. Surg.* **22** (3), 329–333 (2018).
- de Mourão, C. F. Answer controversies about hemostatic properties of platelet-rich fibrin. *Oral Maxillofacial Surg.* **23** (1), 121 (2019).
- de Mourão, C. F. Usefulness of platelet-rich fibrin as a hemostatic agent after dental extractions in patients receiving anticoagulant therapy with factor Xa inhibitors: a case series. *Oral Maxillofac. Surg.* **23** (3), 381–386 (2019).
- de Mourão, C. F. The use of Platelet-rich fibrin in the management of medication-related osteonecrosis of the jaw: A case series. *J. Stomatol. Oral Maxillofac. Surg.* **121** (1), 84–89 (2020).
- Cipitria, A. et al. N. BMP delivery complements the guiding effect of scaffold architecture without altering bone microstructure in critical-sized long bone defects: a multiscale analysis. *Acta Biomater.* **23**, 282–294 (2015).
- NC3Rs Reporting Guidelines Working Group. Animal research: reporting in vivo experiments: the ARRIVE guidelines. *J. Physiol.* **588**, 2519–2521 (2010).
- ISO/TS 22911. *Dentistry – Preclinical Evaluation of Dental Implant systems – Animal Test Methods* (International Organization for Standardization, 2016).
- Sartoretto, S. C. et al. Sheep as an experimental model for biomaterial implant evaluation. *Acta Ortop. Bras.* **24**, 262–266 (2016).
- Scarano, A. et al. Sheep as a preclinical model for dental implant research: bone response and osseointegration assessment. *J. Funct. Biomater.* **15**, 83. <https://doi.org/10.3390/jfb15040083> (2024).
- Kilkenny, C., Brown, W. J., Cuthill, I. C., Emerson, M. & Altman, D. G. Improving bioscience research reporting: the ARRIVE guidelines for reporting animal research. *PLoS Biol.* **8**, e1000412 (2010).
- Smith Aj, C., Re, Lilley, E. & Hansen Kea, Brattelid, T. PREPARE: diretrizes Para O Planejamento de pesquisas e testes Em animais. *Lab. Anim.* **52** (2), 135–141 (2018).
- Sartoretto, S. C. et al. The influence of nanostructured hydroxyapatite surface in the early stages of osseointegration: A multiparameter animal study in Low-Density bone. *Int. J. Nanomed.* **10**, 15:8803–8817 (2020).
- Choukroun, J. et al. Platelet-rich fibrin (PRF): a second-generation platelet concentrate. Part IV: clinical effects on tissue healing. *Oral Surg. Oral Med. Oral Pathol. Oral Radiol. Endod.* **101**, e56–60. <https://doi.org/10.1016/j.tripleo.2005.07.011> (2006).
- Das, S. et al. X-ray computed microtomography datasets for osteogenic nanofibrous coated titanium implants. *Nat. Sci. Data.* **9**, 348. <https://doi.org/10.1038/s41597-022-01400-8> (2022).
- Jones, A. C. et al. Assessment of bone ingrowth into porous biomaterials using MICRO-CT. *Biomaterials* **28**, 2491–2504 (2007).
- Boussein, M. L. et al. Guidelines for assessment of bone microstructure in rodents using Micro-Computed tomography. *J. Bone Miner. Res.* **25** (7Z), 1468–1486 (2010).
- Yurttutan, E., Dereci, Ö. & Karagöz, M. A. Biomechanical and histologic evaluation of osseointegration of titanium dental implants modified by various combinations of sandblasting, acid-etching, hydroxyapatite, and hyaluronic acid coating techniques. *Int. J. Oral Maxillofac. Implants.* **38** (3), 583–590 (2023).

36. Pearce, A. I. et al. Animal models for implant biomaterial research in bone: A review. *Eur. Cells Mater.* **13**, 1–10 (2007).
37. Miron, R. J., Zhang, Y. F., Osteoinduction & A review of old concepts with new standards. *J. Dent. Res.* **91** (8), 736–744 (2012).
38. Kobayashi, E. et al. Comparative release of growth factors from PRP, PRF, and advanced-PRF. *Clin. Oral Invest.* **20** (9), 2353–2360 (2016).
39. Dohan Ehrenfest, D. M. et al. Slow release of growth factors and thrombospondin-1 in Choukroun's platelet-rich fibrin (PRF): a gold standard to achieve for all surgical platelet concentrates technologies. *Growth Factors.* **27** (1), 63–69 (2009).
40. Ondur, E. et al. Effects of Platelet-Rich fibrin on hard tissue healing: A histomorphometric crossover trial in sheep. *Materials* **13** (7), 1695 (2020).
41. Lyris, V., Millen, C., Besi, E. & Pace-Balzan, A. Effect of leukocyte and platelet rich fibrin (L-PRF) on stability of dental implants. A systematic review and meta-analysis. *Br. J. Oral Maxillofacial Surg.* **59** (10), 1130–1139 (2021).
42. Benalcázar Jalkh, E. B. et al. Effect of leukocyte-platelet-rich fibrin in bone healing around dental implants placed in conventional and wide osteotomy sites: A preclinical study. *J. Biomed. Mater. Res. B.* **110** (12), 2705–2713 (2022).
43. Almeida, D. et al. In vivo osseointegration evaluation of implants coated with nanostructured hydroxyapatite in low density bone. *PLoS One.* **18** (2), e0282067 (2023).
44. Mello-Machado, R. C. et al. Osseodensification enables bone healing chambers with improved low-density bone site primary stability: an in vivo study. *Sci. Rep.* **29** (1), 15436 (2021).
45. Luginbuehl, V., Meinel, L., Merkle, H. P. & Gander, B. Localized delivery of growth factors for bone repair. *Eur. J. Pharm. Biopharm.* **58** (2), 197–208 (2004).
46. Al-Musawi, M. H. et al. Localized delivery of healing stimulator medicines for enhanced wound treatment. *J. Drug Deliv. Sci. Technol.* **101**, 106212 (2024).
47. Ribeiro, E. D. et al. The efficacy of platelet and leukocyte rich fibrin (L-PRF) in the healing process and bone repair in oral and maxillofacial surgeries: a systematic review. *Oral Investigations.* **28** (7), 414 (2024).

Acknowledgements

The authors thank Prof. Helder Valliense for helping to create the schematic figure (Figure 1).

Author contributions

M.D.C.-M.; E.J.B.B. and B.G.: Study design and manuscript preparation. M.D.C.-M.; S.C.S.; S.M.; F.L.: Surgical Intervention. M.D.C.-M.; J.M.G.: preparation and submission of the manuscript. P.S.N.; M.D.C.-M.; S.C.S.: Histological and histomorphometric evaluation. S.M.; F.L.; J.G.M.; C.M.S.F.F.S.; interpretation of the results and preparation of the materials. J.M.G. and M.D.C.-M.: Supervise and prepare the manuscript. C.M.S.F.F.S.; microtomographic evaluation. All authors have read, edited, and approved the final manuscript.

Funding

This study was financed by S.I.N. Implant System, Sao Paulo, Brazil, but the company had no influence in the design, execution, and analysis of the results. Faperj: Protocol # 26/010.002989/2014; Protocol # E-26/010.0000981/2019; E-26/200.321/2023. CNPq: Protocol # 308156/2020-0; Protocol #422783/2021-8.

Declarations

Competing interests

The authors declare no competing interests.

Additional information

Correspondence and requests for materials should be addressed to J.M.G.

Reprints and permissions information is available at www.nature.com/reprints.

Publisher's note Springer Nature remains neutral with regard to jurisdictional claims in published maps and institutional affiliations.

Open Access This article is licensed under a Creative Commons Attribution-NonCommercial-NoDerivatives 4.0 International License, which permits any non-commercial use, sharing, distribution and reproduction in any medium or format, as long as you give appropriate credit to the original author(s) and the source, provide a link to the Creative Commons licence, and indicate if you modified the licensed material. You do not have permission under this licence to share adapted material derived from this article or parts of it. The images or other third party material in this article are included in the article's Creative Commons licence, unless indicated otherwise in a credit line to the material. If material is not included in the article's Creative Commons licence and your intended use is not permitted by statutory regulation or exceeds the permitted use, you will need to obtain permission directly from the copyright holder. To view a copy of this licence, visit <http://creativecommons.org/licenses/by-nc-nd/4.0/>.

© The Author(s) 2025